Post-Print

This is the accepted version of:

Scalar mixing in homogeneous isotropic turbulence:
a numerical study

Michel Orsi,[1] Lionel Soulhac,[2] Fabio Feraco,[2,3] Massimo Marro,[2]

Duane Rosenberg,[4] Raffaele Marino,[2] Maurizio Boffadossi,[1] and Pietro Salizzoni[2]

[1]*Department of Aerospace Engineering,*

Politecnico di Milano, 34 via La Masa, 20158 Milano, Italy

[2]*Laboratoire de Mécanique des Fluides et d'Acoustique,*

University of Lyon, CNRS UMR 5509, École Centrale de Lyon,

INSA Lyon, Université Claude Bernard,

36 avenue Guy de Collongue, 69134 Écully, France

[3]*Dipartimento di Fisica, Università della Calabria, Italy*

[4]*1401 Bradley Drive, 80305 Boulder CO, USA*

(Dated: March 6, 2021)

Abstract

The understanding of the mechanics of turbulent dispersion is of primary importance in estimating the effects of mixing processes involved in a variety of events playing a significant role in our daily life. This motivates research on the characterisation of statistics and the complex temporal evolution of passive scalars in turbulent flows. A key aspect of these studies is the modelling of the probability density function (PDF) of the passive scalar concentration and the identification of its link with the mixing properties. In order to investigate the dynamics of passive scalars, as observed in nature and in laboratory experiments, we perform here direct numerical simulations (DNS) of a passive tracer injected in the stationary phase of homogeneous isotropic turbulence (HIT) flows, in a setup mimicking the evolution of a fluid volume in the reference frame of the mean flow. In particular, we show how the gamma distribution proves to be a suitable model for the PDF of the passive scalar concentration and its temporal evolution in a turbulent flow throughout the different phases of the mixing process. Then, assuming a gamma distribution, we develop a simple mixing model by which we can estimate a mixing time scale, which regulates the decay rate of the intensity of the concentration fluctuations.
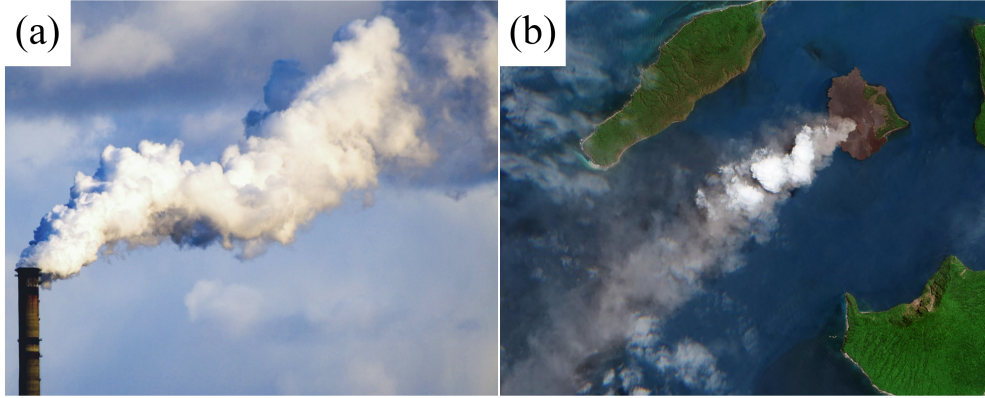
FIG. 1. Plume generated by a chimney (i.e., an elevated continuous source in a non-isotropic and non-homogeneous turbulent flow field) (a); volcanic ash and steam in the Sunda Strait released by Anak Krakatau volcano in Indonesia three months before its eruption in December 2018 (b).

I. INTRODUCTION

Turbulent dispersion and mixing of passive scalars are ubiquitous in nature. As it is well known, the turbulent character of high Reynolds number flows is reflected on the fluctuations of the passive scalar concentration occurring over a wide range of spatial and temporal scales [1]. The statistical characterisation of these fluctuations is essential for the modelling of several processes occurring in industrial, biological, and environmental flows (see Figure 1 as examples). To this aim, over the years this issue has been tackled by several authors considering a large variety of flow configurations [2–8].

In a number of applications of interest in physics, chemistry, biology, and engineering, a key aspect is the prediction of the spatial variability of the one-point PDF of the scalar field. Previous works have shown that, depending on the flow configuration, this can be modelled by different distributions [2–9], including the Weibull, the lognormal, and the gamma distributions. Notably, the latter was shown to be a suitable model for both dispersion and mixing in internal flows [2–7] and in the atmosphere [6–8, 10–14].

The present work aims at further exploring the above features, through the investigation of concentration statistics and mixing in a framework mimicking the evolution of the passive scalar in a homogeneous isotropic turbulent flow. To this purpose, we performed DNS of a stationary turbulent velocity field (with zero mean) where a puff of passive scalar was released and let evolve to get insights on its diffusion and mixing properties (Section II). In

2

Section III concentration statistics and PDF computed on the point-wise simulated fields were first checked to ascertain their reliability and, then, linked to the main mechanisms involving the mixing. Finally, we discuss the consistency between spatial statistics computed by the DNS (seeing the puff as evolving in a Lagrangian framework moving with the mean flow) and the temporal statistics based on one-point wind-tunnel measurements (Section IV).

II.   NUMERICAL SIMULATION

In order to investigate the dispersion and mixing of a passive scalar in HIT, the Navier-Stokes equations for an incompressible fluid together with the convection-diffusion equation for the concentration are integrated by means of the Geophysical High-Order Suite for Turbulence (GHOST) code [15], a highly parallelised (hybrid MPI-OpenMP) pseudo-spectral framework with second order explicit Runge-Kutta time stepping. The Navier-Stokes equations have been integrated on a cubic grid of 512^3 points (corresponding to a box whose linear size in adimensional units is $L_0 = 2\pi$), with periodic boundary conditions. A stochastic forcing $\mathbf{F}$ was used to inject energy into the velocity field to achieve and maintain a statistically stationary state. The forcing is random in time and isotropic in Fourier space, with the energy being injected at large scales in a spherical shell of wavenumbers $2 \leq |k_i| \leq 3$. A puff of passive scalar modelled with a Gaussian concentration peaked in the centre of the box is injected at an arbitrary time in the statistically stationary state of the simulation and is let to diffuse. The full system of equations implemented is reported here:

$$\begin{cases} \nabla \cdot \mathbf{u} = 0, \\ \partial_t \mathbf{u} + (\mathbf{u} \cdot \nabla)\mathbf{u} = -\nabla p + \mathbf{F} + \dfrac{1}{Re}\nabla^2 \mathbf{u}, \\ \partial_t c + \mathbf{u} \cdot \nabla c = \dfrac{1}{PrRe}\nabla^2 c, \end{cases} \tag{1}$$

$\mathbf{u}$ being the velocity field, p the pressure, and c the passive scalar concentration. The DNS governing parameters are the Prandtl (Pr) and the Reynolds (Re) numbers. The former, defined as $Pr \equiv \nu/\kappa$, is set equal to 1 (being ν and κ the kinematic viscosity and the diffusivity, respectively). The latter is instead $Re \equiv \frac{UL}{\nu}$, where $U = \sqrt{3\sigma_u^2}$ (being $\sigma_u^2 = \sigma_v^2 = \sigma_w^2 \sim 1$ the variances of the 3 velocity components averaged over the computational domain) and $L = \frac{2\pi}{k_i \sim 2.5}$ are respectively the characteristic velocity and the integral length scale of the background fluid (the latter being estimated as the scale at which energy is injected
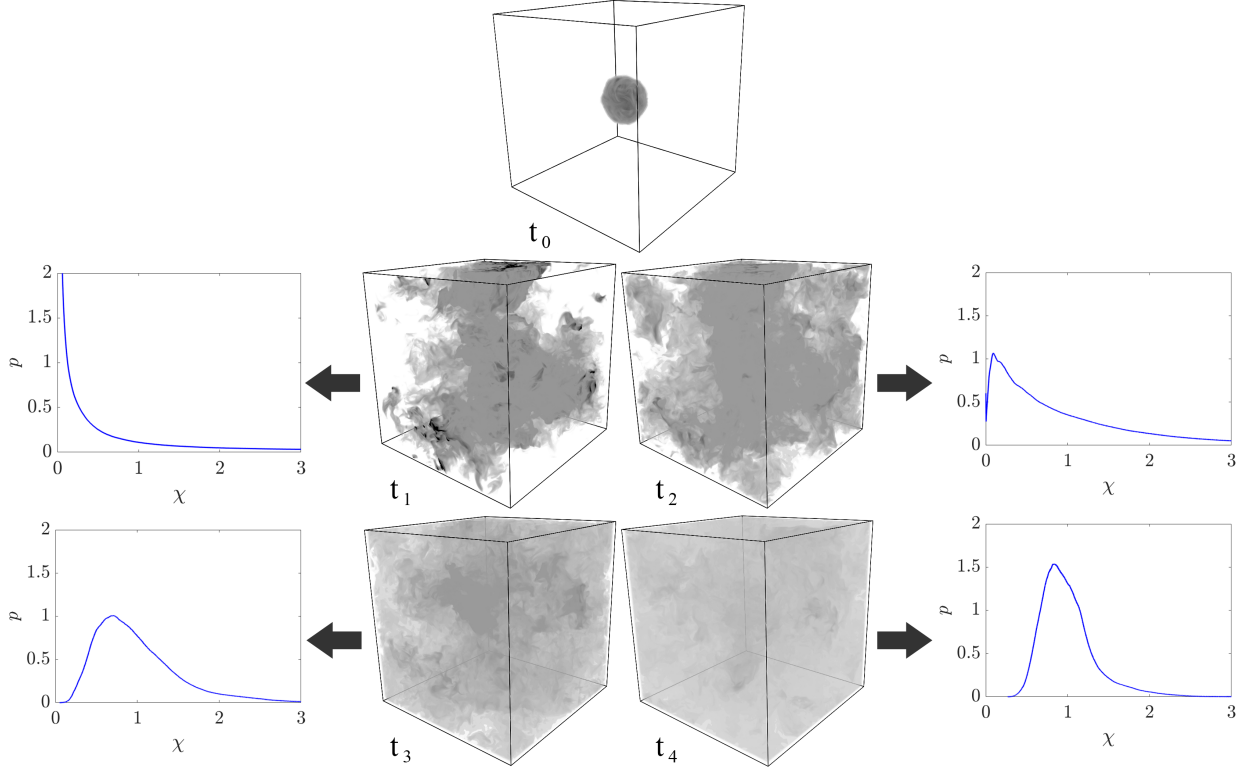
3

FIG. 2. Visualisation of different instants of the DNS solutions and corresponding concentration PDFs: at the top (t_0), the initial condition can be observed; at the bottom right (t_4), the passive scalar homogenises itself within the box.

into the system). Based on these quantities we can estimate the turnover time $t^* \equiv L/U$, the characteristic time scale of the simulation, whose total extension is about $10\,t^*$. The simulations have been performed at two Reynolds numbers, namely 3000 and 3500. For $Re = 3000$ the Kolmogorov length scale is $\eta = (\nu^3/\varepsilon)^{1/4} = 8.15 \times 10^{-3}$ (ε is the turbulent kinetic energy dissipation rate), which is three order of magnitude lower than the integral length scale ($\eta/L = 3.24 \times 10^{-3}$). Note that the (periodic) boundary conditions induce the concentration averaged over the domain ($\bar{c}$) to be constant throughout the simulation duration.

III.   RESULTS

The concentration statistics provided by the DNS results allow the temporal evolution of the mixing process to be investigated. To that purpose, we focus on two main statistical
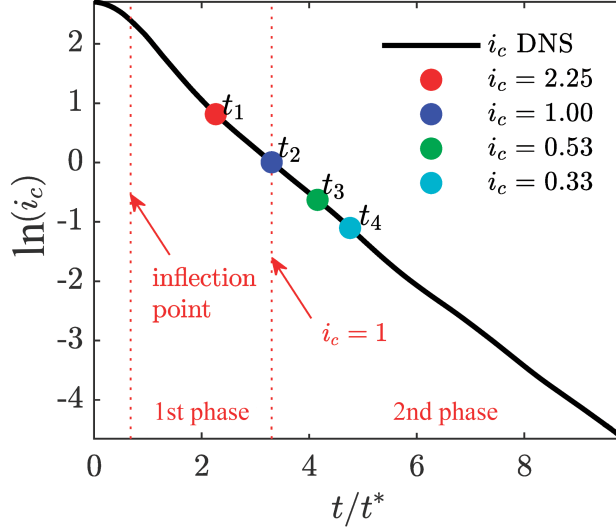
FIG. 3. Behaviour of the concentration fluctuations intensity i_c over time: four instants t_1, t_2, t_3, and t_4 are highlighted.

indicators: the shape of the PDF of the spatial distribution of the concentration and the (volume averaged) concentration fluctuations intensity i_c (defined as the ratio between the standard deviation of the concentration σ_c and $\bar{c}$). The first feature that is worth noting is the strict connection between the temporal evolution of these two indicators.

Notably, once excluded the early transient of the simulation (lasting less than one turnover time t^*) during which the system progressively "looses memory" of the initial concentration distribution (Figure 2, t_0), we can identify two main stages of the process, by linking the shape of the PDFs (Figure 2) to i_c (Figure 3). To allow the reader to suitably capture this connection between the concentration PDF and i_c, we provided a movie as Supplemental Material [16]. During the first phase, starting at the inflection point of i_c, the scalar is progressively transported throughout the domain, as shown in Figure 2 at t_1. This stage presents specific features: i) i_c is larger than 1, ii) the concentration PDF is characterised by a large number of zero-values (mostly distributed at the edge of the evolving puff), and iii) it approximates an exponential-like shape. The second phase begins when the domain gets completely filled by the passive scalar (Figure 2 at t_2) and $i_c = 1$ (Figure 3), and it is mostly characterised by the diffusion. During this stage the scalar field progressively homogenises (as shown in Figure 2 at t_3) and the concentration PDFs assume a lognormal-like shape. The increasing scalar homogenisation (Figure 2 at t_4) induces a further transition of the

PDFs towards a clipped Gaussian [13].

The results of the simulations performed with two different Reynolds number (i.e., $Re = 3000$ and $Re = 3500$) did not show any relevant difference one to the other. In what follows we will therefore presents results for the case $Re = 3000$. ncentration statistics recover those obtained with the smaller blob as $t/t^* > 2$.

A. Concentration PDF

In order to identify the statistical distribution showing the best agreement with the presented numerical results, we tested different models for the scalar PDF. To do this, we therefore computed the PDF of the concentration for each time step. The agreement between the PDFs obtained from the DNS and the analytical model distributions is estimated here using the Kullback-Leibler divergence D_{KL} [17], defined as:

$$D_{KL}(p \parallel q) \equiv -\sum p \, \log_2 \left(\frac{p}{q} \right), \tag{2}$$

where p is the PDF from the DNS, q is the distribution assumed as model. According to this definition, the best agreement is observed when $p/q \to 1$, i.e. for $D_{KL} \to 0$.

We tested three different distributions which have been proposed over the years as suitable models for the passive scalar concentration PDF within a turbulent flow [2–9]. These are:

- the gamma distribution:

$$p(\chi|\lambda, \theta) = \frac{1}{\Gamma(\lambda)\theta} \left(\frac{\chi}{\theta} \right)^{\lambda-1} \exp\left(-\frac{\chi}{\theta} \right), \tag{3}$$

where χ is the sample space variable for the concentration, $\Gamma(\cdot)$ is the Gamma special function [18], and $\lambda = i_c^{-2}$ and $\theta = \sigma_c^2/\overline{c}$ are the shape and scale parameters, respectively. It is worth noting that normalising the distribution as $\chi' \equiv \chi/\overline{c}$ allows us to reduce the problem to only the shape parameter λ [2, 19, 20];

- the lognormal distribution:

$$p(\chi|\mu_l, \sigma_l) = \frac{1}{\chi\sigma_l\sqrt{2\pi}} \exp\left[-\frac{(\ln \chi - \mu_l)^2}{2\sigma_l^2} \right], \tag{4}$$

for $\chi > 0$ and with the parameters:

$$\mu_l = \ln \left(\overline{c}^2 / \sqrt{\sigma_c^2 + \overline{c}^2} \right),$$
$$\sigma_l = \sqrt{\ln \left(\sigma_c^2/\overline{c}^2 + 1 \right)}; \tag{5}$$
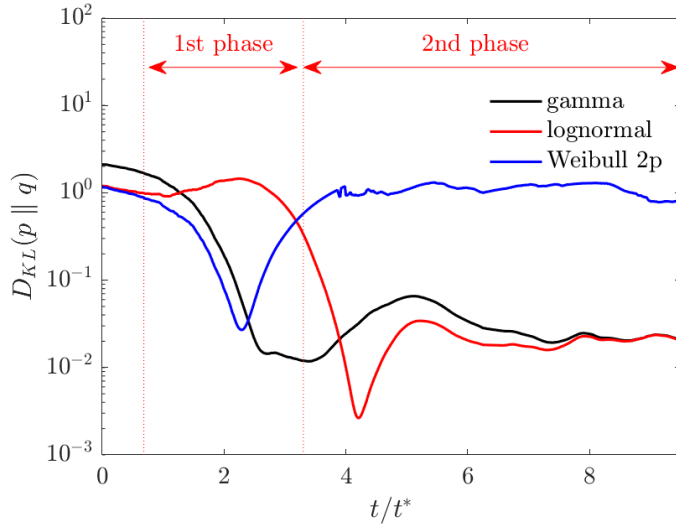
6

FIG. 4. Kullback-Leibler divergence of the PDF from the DNS results (semi-logarithmic plot): comparison between the gamma, the lognormal, and the Weibull 2p distributions. The two vertical dashed lines indicate different phases of the mixing processes, as defined in Section III. The KL divergence of the gamma distribution presents a good overall behaviour and it is the most suitable choice for modelling the scalar-field PDF for all the time steps.

- the Weibull 2p distribution:

$$p(\chi|a_w, b_w) = \frac{b_w}{a_w} \left(\frac{\chi}{a_w}\right)^{b_w-1} \exp\left[-\left(\frac{\chi}{a_w}\right)^{b_w}\right], \qquad (6)$$

being a_w and b_w the scale and the shape parameters, respectively, set as:

$$i_c^2 + 1 - \frac{\Gamma\left(1 + \frac{2}{b_w}\right)}{\left[\Gamma\left(1 + \frac{1}{b_w}\right)\right]^2} = 0,$$

$$a_w = \frac{\overline{c}}{\Gamma\left(1 + \frac{1}{b_w}\right)}. \qquad (7)$$

We point out that the computation of b_w requires to solve the non-linear Eq. 7. We mention that for practical application the shape parameters can be conveniently approximated as $b_w \approx (1/i_c)^{1.086}$ [e.g., 21].

As shown in Figure 4, close to t_0 the lognormal distribution is not appropriate since it is not able to reproduce the effects of the meandering process in the near-field, as observed close to the scalar source in wind-tunnel experiments. Conversely, it provides accurate estimates

of the scalar PDF after the homogenisation process induced by the relative dispersion. The Weibull 2p distribution performs suitable approximations of the concentration PDF in the near-field, whereas it fails to model the distribution of the scalar at large values of t/t^*.

The gamma distribution shows a more accurate overall behaviour providing a good agreement with the numerical solutions both in the near and in the far field. Such behaviour suggests that the gamma PDF is a robust model being able to replicate the main features of the mixing process over the entire DNS.

B. Mixing

As a second step, we discuss here the implications of a mixing process due to the interaction of pollutant particles, assuming, based on the results presented in the previous paragraph, that the PDF of the concentration within our reference volume is a gamma distribution. In order to analyse the mixing process, we focus on the fluctuations intensity i_c, that progressively goes to zero. Note that, because of the imposed boundary conditions (Section II), the decay of i_c is entirely due to the reduction of the standard deviation σ_c, since the spatially averaged concentration $\bar{c}(t)$ remains unaltered.

We represent the passive-scalar puff as constituted of an ensemble of "marked" fluid particles, so that the mixing process is modelled as a "discrete" phenomenon resulting by the interaction of pairs of marked fluid particles. This is a classical pattern in PDF methods for the prediction of concentration fluctuations (referred as micromixing models) implemented in Lagrangian one-particle dispersion models [9, 22]. In this kind of models, each fluid particle exchanges mass with the surrounding particles and, as a consequence, the concentration statistics defined by an ensemble of neighbouring particles evolve in time. Then, following this analogy, the concentrations of the fluid particles can be considered as single realisations of the same random variable whose statistical behaviour is modelled by a distribution that we assume to be a gamma PDF. The two fluid particles, denoted as '1' and '2', exchange mass each other, so that the temporal evolution of their concentrations develops as a system of two ordinary differential equations:

$$\begin{cases} \dfrac{dc_1}{dt} = -\dfrac{c_1 - c_2}{\tau_m}, \\ \dfrac{dc_2}{dt} = -\dfrac{c_2 - c_1}{\tau_m}, \end{cases} \tag{8}$$

8

where τ_m is the characteristic time scale of the mixing process. The solution of the system above in the time interval $[t', t' + \Delta t]$ is:

$$\begin{cases} c_1(t' + \Delta t) = (1 - \alpha) \, c_1(t') + \alpha \, c_2(t'), \\ c_2(t' + \Delta t) = \alpha \, c_1(t') + (1 - \alpha) \, c_2(t'), \end{cases} \tag{9}$$

where:

$$\alpha \equiv \frac{1}{2} \left[1 - \exp\left(-2\frac{\Delta t}{\tau_m} \right) \right]. \tag{10}$$

Generalising this approach to any pair of fluid particles i and j within the domain, we conclude that predicting the effect of mixing is equivalent to estimate the PDF of a new random variable c_k given by a weighted sum of c_i and c_j:

$$c_k(t' + \Delta t) = (1 - \alpha)c_i(t') + \alpha c_j(t'). \tag{11}$$

The PDF of c_k is then given by the convolution of the PDFs for c_i and c_j. Since $c_i(t')$ and $c_j(t')$ are both distributed according to the same gamma PDF $p(\lambda, \theta)$, we have that:

$$\begin{cases} (1 - \alpha) \, c_i(t') & \text{follows} \quad p_i(\lambda, (1 - \alpha)\theta), \\ \alpha \, c_j(t') & \text{follows} \quad p_j(\lambda, \alpha\theta). \end{cases} \tag{12}$$

As far as we are aware, simple expressions for the convolution of two gamma distributions having different scale parameters (as in Eq. 12) are not known. Moschopoulos [23] and Sim [24] provided the exact convolution as a sum of infinite terms, and Mathai [25] and Akkouchi [26] proposed some complicated formulas. An alternative approach was investigated in Stewart et al. [27] who showed that the sum of gamma PDFs is suitably approximated by a gamma distribution if the scale parameters differ no more than a factor of 10 and the shape parameters are not below 0.1. In our case these conditions are generally satisfied. The first condition is fulfilled for $\Delta t \geq 0.2 \, \tau_m$, and the second one for $i_c \lesssim 3.2$. Therefore, the PDF $p_k(\lambda_k, \theta_k)$ of c_k (Eq. 11) is suitably approximated as a gamma distribution [27] and its scale and shape parameters can be determined by computing mean and variance as follows:

$$\begin{aligned} \bar{c}_k &= \lambda_k \theta_k = \lambda(1 - \alpha)\theta + \lambda\alpha\theta = \lambda\theta, \\ \sigma_{c,k}^2 &= \lambda_k \theta_k^2 = \lambda(1 - \alpha)^2\theta^2 + \lambda\alpha^2\theta^2 = \lambda\theta^2[(1 - \alpha)^2 + \alpha^2], \\ \theta_k &= \frac{\sigma_{c,k}^2}{\bar{c}_k} = \theta \left[\alpha^2 + (1 - \alpha)^2 \right], \\ \lambda_k &= \frac{\bar{c}_k^2}{\sigma_{c,k}^2} = \frac{\lambda}{\alpha^2 + (1 - \alpha)^2}. \end{aligned} \tag{13}$$

9

As a consequence of the mixing process, the first two moments of the concentration PDF evolve as (dropping the indexes for clarity):

$$\bar{c}(t' + \Delta t) = \bar{c}(t'),$$
$$\sigma_c^2(t' + \Delta t) = \beta \sigma_c^2(t'), \tag{14}$$

where:

$$\beta \equiv \alpha^2 + (1 - \alpha)^2 = \frac{1}{2}\left[1 + \exp\left(-4\frac{\Delta t}{\tau_m}\right)\right]. \tag{15}$$

Performing a limited development of this process for short intervals and neglecting the higher-order terms, we obtain the evolution of the characteristics of the distribution between t' and $t' + \Delta t$:

$$\bar{c}(t' + \Delta t) = \bar{c}(t')$$
$$\sigma_c^2(t' + \Delta t) = \left(1 - 2\frac{\Delta t}{\tau_m}\right)\sigma_c^2(t'). \tag{16}$$

Since Eq. 16 represents the incremental ratio of σ_c, we can write the time derivative of the concentration variance as:

$$\lim_{\Delta t \to 0} \frac{\sigma_c^2(t' + \Delta t) - \sigma_c^2(t')}{\Delta t} = \frac{d\sigma_c^2}{dt} = -\frac{2}{\tau_m}\sigma_c^2. \tag{17}$$

which essentially expresses the dissipation rate of the scalar variance $\varepsilon_c \equiv -2\nu \left\langle \partial c'/\partial x_i \right\rangle^2$.

The above expression can be integrated in order to obtain the temporal evolution of σ_c^2:

$$\sigma_c^2(t) = \sigma_c^2(0) \exp\left(-2\frac{t}{\tau_m}\right), \tag{18}$$

and therefore:

$$\sigma_c(t) = \sigma_c(0) \exp\left(-\frac{t}{\tau_m}\right). \tag{19}$$

Since we have $\bar{c}(t) = \bar{c}(0)$, we finally obtain that the temporal decay of i_c evolves as:

$$i_c(t) = i_c(0) \exp\left(-\frac{t}{\tau_m}\right), \tag{20}$$

showing that the assumption of the gamma distribution for the concentration PDF implies that the fluctuations intensity is given by a negative exponential, whose decay is governed by a typical mixing time scale.

The mixing time scale τ_m can be estimated from our numerical experiments by locally fitting Eq. 20 (i.e., over short intervals) with the DNS results for i_c, having τ_m as free parameter (evolving in time). Once excluded the initial transient ($t/t^* < 1$), this time scale
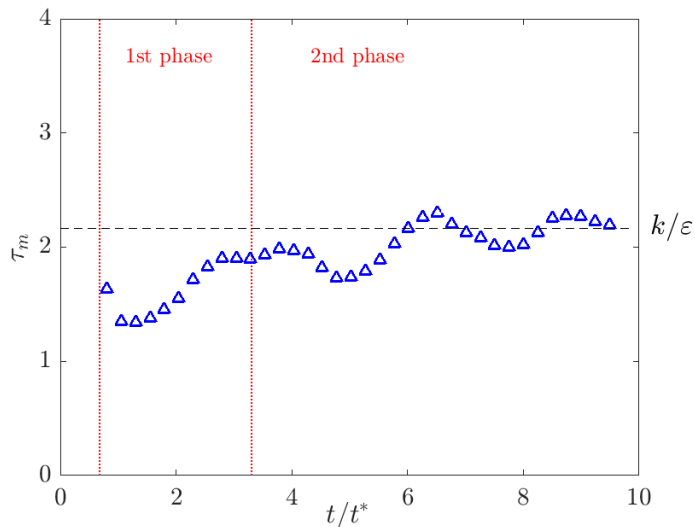
FIG. 5. Mixing time scale τ_m vs t/t^*. In the far field τ_m reaches the asymptotic value of k/ε.

exhibits a smoothly growing trend in the first phase and oscillates around a constant value in the second phase. At later times, in the second phase of the simulation τ_m attains an asymptotic value equal to the dissipative time scale $\tau \equiv k/\varepsilon$ (where $k \equiv \frac{3}{2}\sigma_u^2$ is the turbulent kinetic energy and $\varepsilon \equiv 2\nu \langle s_{ij}s_{ij}\rangle$ is its dissipation rate) [28, 29], as pointed out in Figure 5. We highlight that the numerical results show that for large values of t/t^* the ratio $\tau/\tau_m \approx 1$, which is in agreement with the findings of other authors that reported values in the range 0.3–1.56 for different configurations [22, 30–33].

IV. ANALOGIES WITH WIND-TUNNEL RESULTS AND CROSS-VALIDATION OF THE GAMMA MODEL

In Section III we have shown the temporal evolution of the normalised PDF of the passive scalar concentration and pointed out its link with the value of i_c: the shape of the PDF exhibits an exponential-like form as far as $i_c > 1$, it abruptly changes shape for $i_c = 1$ and evolves as a Gaussian-like distribution as $i_c \to 0$. This same behaviour, observed here adopting statistics over a control fluid volume for each time step, was observed in wind-tunnel experiments when analysing one-point statistics obtained from concentration time series measured at a fixed location downwind a continuous scalar release in a turbulent boundary layer, as described in [13]. Indeed, wind-tunnel experiments have shown that
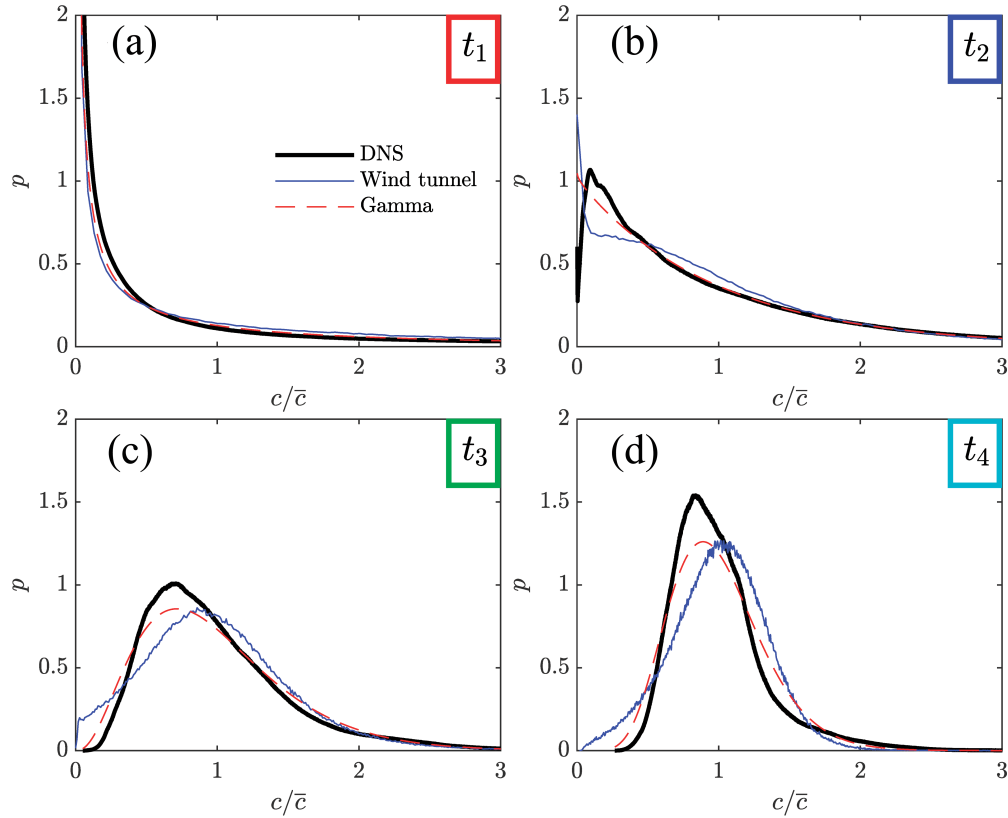
FIG. 6. Comparison between the normalised PDFs of the passive scalar concentration from the DNS, the wind-tunnel measurements by Nironi et al. [13], and the gamma distribution of Eq. 3 at decreasing values of i_c: (a) $i_c = 2.25$ at t_1, (b) $i_c = 1$ at t_2, (c) $i_c = 0.53$ at t_3, (d) $i_c = 0.33$ at t_4.

the statistics of the concentration of a continuous scalar plume in a boundary layer (i.e., a non-isotropic and non-homogeneous velocity field) can be fully described by a gamma distribution as reported in Eq. 3.

In Figure 6 we show a comparison between the present DNS results, the one-point wind-tunnel statistics performed by Nironi et al. [13] and the gamma distribution (Eq. 3) for the same values of i_c (being t_1, t_2, t_3, t_4 the same as in Figure 3). Here, we can appreciate how the DNS solutions and the wind-tunnel measurements exhibit a similar behaviour and that the gamma distribution can be assumed as a suitable model for both numerical and experimental PDFs. To explain this evidence from a phenomenological stand point, we can rely on the depiction in Figure 7, proposing the analogy between the present DNS simulation of an unsteady decaying puff and the wind-tunnel results of a steady release of a passive scalar in a turbulent wall-bounded flow.
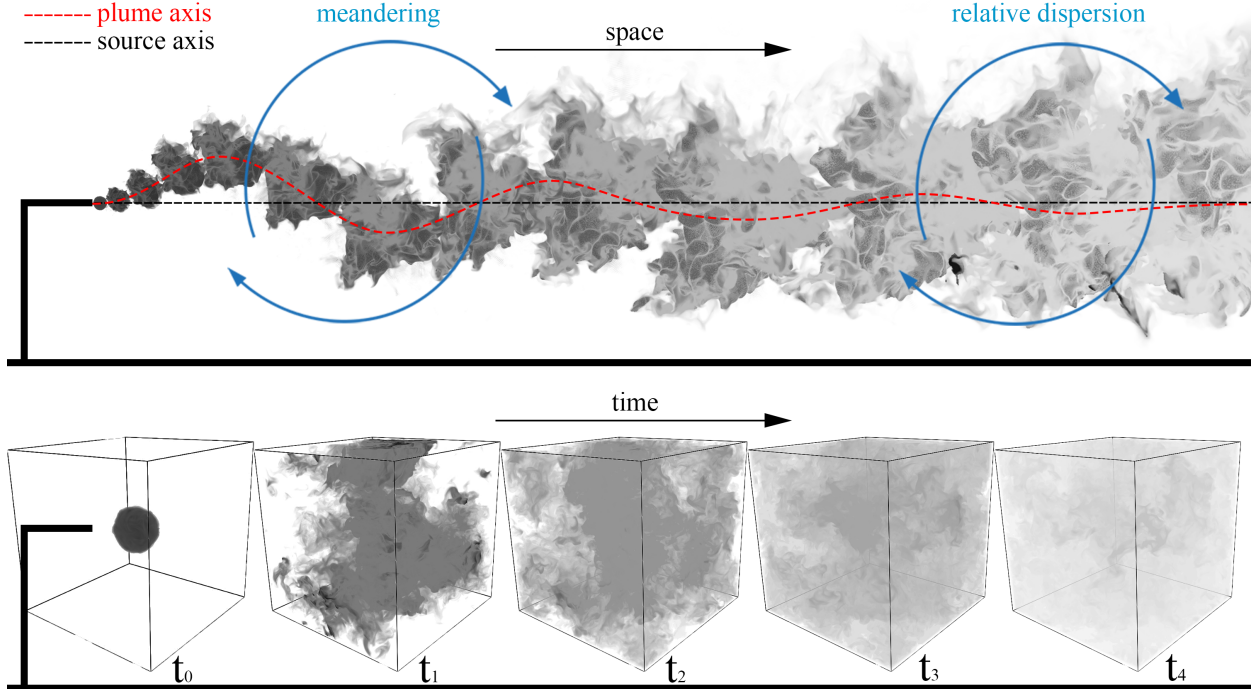
FIG. 7. Top panel: sketch of a plume as made of multiple puffs, Eulerian approach. Bottom panel: numerical point of view, Lagrangian approach. We observe the relationship between *space* and *time* in the two different approaches, as well as the regions of *meandering* and *relative dispersion*.

A peculiar aspect of the dispersion of localised atmospheric releases is the appearance of a meandering motion of the plume [12], due to the action of turbulent eddies larger than the plume size. The meandering highly affects the dispersion process in the near field of the source and is gradually attenuated moving away from it, as the size of the plume increases under the action of the relative dispersion (due to eddies smaller than the puff size). As the relative dispersion finally induces the plume size to exceed the size of the larger scale structure of the flow, the plume meandering is suppressed. At first sight, we can consider that the transition between these two regimes occurs as i_c drops below 1 and the intermittency is suppressed in the core of the plume [13].

In the puff, at each time step, every point of the simulation domain can be considered as a possible realisation of the plume along the source axis at a given distance from the source, in the equivalent reference wind-tunnel experiment. In other words, we can consider that the DNS results mimic the evolution of the scalar puffs released in the wind tunnel as they get translated horizontally by the mean flow while undergoing turbulent advection.

Invoking the ergodicity of both numerical and experimental flows, we could therefore compare the spatial statistics computed on the simulation output (Figure 7 bottom) with the single-point temporal statistics computed in the wind tunnel (Figure 7 top). Thus, taking a specific instant of the DNS, the spatial statistics of the concentration over the entire simulation box would match the temporal statistics of the concentration signal measured at the corresponding position (always on the plume centreline, i.e. at the source height) in the wind-tunnel experiment. In this framework, the near-source meandering region in the experiments (Figure 7 top panel), in which one-point statistics exhibit high intermittency, corresponds to the first phase of the DNS simulation (Figure 7 bottom panel, t_1), in which the scalar has not filled the domain yet and the spatial concentration statistics are affected by the presence of zero-values of the concentration in part of it. Similarly, the far-field relative dispersion region, in which the intermittency in the one-point statistics is suppressed, corresponds to the second phase of our DNS results (Figure 7 bottom panel, t_3 and t_4), in which the scalar has filled the box and the mixing acts towards a complete homogenisation of the concentration.

In the description of the dispersion process made so far, we adopted a jargon familiar to researchers working in the field of the atmospheric pollutant dispersion. Other researcher working reactive and non-reactive scalar mixing in turbulent flows adopt a different terminology to identify different regimes of the time evolution of the tracer distribution. According to this terminology, the second phase of our numerical simulations shows a behaviour similar to that of the "confined mixture" regime in which, following Duplat and Villermaux [7], a self-convolution mechanism leads to a sequence of gamma distributions until complete mixing is reached. The dispersion in the near-source region where the plume meanders in an unbounded environment has been instead referred as "ever dispersion mixture" by Duplat et al. [34]. The near-source region investigated by Duplat et al. [34] is however more similar to the initial transient of our simulations, in which the concentration PDFs are not consistent with the gamma model (see Figure 2 between t_0 and t_1), rather than what we referred to as the first-phase, where gamma model actually holds. Similar considerations about the lack of accuracy of the gamma distribution as a model for the concentration PDFs very close to the release point were also presented by Sawford and Stapountzis [35] and Ardeshiri et al. [14].

V. CONCLUSIONS

We employed direct numerical simulations to investigate the passive-scalar dispersion and the related mixing processes within turbulent flows in a synergistic approach that involved the use of wind-tunnel measurements for the cross-validation (numerical and experimental) of the gamma model for the scalar distribution concentration. In particular, we simulated a single puff in homogeneous isotropic turbulence in a cubic domain with a regular grid and periodic boundary conditions.

Focus of our work is the analysis of the evolution in time of the spatial statistics of the scalar concentration within a fluid volume as seen in a reference frame following the mean flow. As first step, we tested the capability of different model distributions (the gamma, the lognormal, and the Weibull 2p) in reproducing the spatial PDF of the concentration showing that the gamma distribution is the most robust and convenient model to describe the whole temporal evolution of the dispersion process. Assuming the gamma distribution as the PDF describing the scalar concentration within a given volume, we developed a simple probabilistic mixing model, that allows us to link the decay rate of the intensity of the concentration fluctuations i_c to a characteristic mixing time scale.

Finally, drawing an analogy between the present DNS results and previous experimental data allows us to explain the similarity observed between the spatial statistics in the system considered here and the one-point statistics registered in wind-tunnel experiments. Notably, the first phase of the simulations provides a PDF that can be observed in wind-tunnel experiments by registering the concentration signal close to the source, when the meandering of the plume is intense. Instead, in the second phase of the simulation, when the scalar has filled the whole domain, the concentration PDF corresponds to experimental PDF registered far from the source, where the plume meandering is suppressed and the plume spread is governed by the relative dispersion.

A comparison between DNS and wind-tunnel measurements of stratified turbulence will be the subject of a future investigation along the lines of the present work. Indeed, unlike the HIT case, in presence of stratification, sporadic extreme events develop in the vertical component of the velocity and in the temperature affecting mixing and transport properties of turbulent flows as shown in previous works [36–39].

---

[1] K. R. Sreenivasan, Turbulent mixing: A perspective, Proc. Nat. Acad. Science , 201800463 (2018).

[2] E. Villermaux and J. Duplat, Mixing as an aggregation process, Phys. Rev. Lett. **91**, 184501 (2003).

[3] J. Bakosi, P. Franzese, and Z. Boybeyi, Probability density function modeling of scalar mixing from concentrated sources in turbulent channel flow, Phys. Fluids **19**, 115 (2007).

[4] Q. Nguyen and D. V. Papavassiliou, A statistical model to predict streamwise turbulent dispersion from the wall at small times, Phys. Fluids **28**, 125103 (2016).

[5] P. R. Van Slooten, Jayesh, and S. B. Pope, Advances in pdf modeling for inhomogeneous turbulent flows, Phys. Fluids **10**, 246 (1998).

[6] E. Yee and A. Skvortsov, Scalar fluctuations from a point source in a turbulent boundary layer, Phys. Rev. E **84**, 036306 (2011).

[7] J. Duplat and E. Villermaux, Mixing by random stirring in confined mixtures, J. Fluid Mech. **617**, 51 (2008).

[8] D. J. Wilson and B. W. Simms, Exposure time effects on concentration fluctuations in plumes (Alberta Environment, 1985).

[9] M. Cassiani, The volumetric particle approach for concentration fluctuations and chemical reactions in Lagrangian particle and particle-grid models, Boundary-Layer Meteorol. **146**, 207 (2013).

[10] M. Bertagni, M. Marro, P. Salizzoni, and C. Camporeale, Solution for the statistical moments of scalar turbulence, Phys. Rev. Fluids **4**, 124701 (2019).

[11] M. Bertagni, M. Marro, P. Salizzoni, and C. Camporeale, Level-crossing statistics of a passive scalar dispersed in a neutral boundary layer, Atmospheric Environment **230**, 117518 (2020).

[12] M. Cassiani M., Bertagni, M. Marro, and P. Salizzoni, Concentration fluctuations from localized atmospheric releases, Boundary-Layer Meteorology **177**, 461 (2020).

[13] C. Nironi, P. Salizzoni, M. Marro, P. Mejean, N. Grosjean, and L. Soulhac, Dispersion of a pas-

sive scalar fluctuating plume in a turbulent boundary layer. Part I: Velocity and concentration measurements, Boundary-Layer Meteorol. **156**, 415 (2015).

[14] H. Ardeshiri, M. Cassiani, S. Park, A. Stohl, I. Pisso, and S. Dinger, On the convergence and capability of large eddy simulation for passive plumes concentration fluctuations in an infinite-Re neutral boundary layer, Boundary-Layer Meteorol. **176**, 291 (2020).

[15] P. D. Mininni, D. Rosenberg, R. Reddy, and A. Pouquet, A hybrid mpi-openmp scheme for scalable parallel pseudospectral computations for fluid turbulence, Parallel Computing **37**, 316 (2011).

[16] See supplemental material at [url will be inserted by publisher] to suitably capture the connection between the concentration pdf and the concentration fluctuations intensity i_c.

[17] S. Kullback and R. A. Leibler, On information and sufficiency, The Annals of Mathematical Statistics **22**, 79 (1951).

[18] M. Abramowitz and I. A. Stegun, Handbook of mathematical functions: with formulas, graphs, and mathematical tables (Nat. Bur. of Standards Appl. Math., 1965).

[19] E. Yee and R. Chan, A simple model for the probability density function of concentration fluctuations in atmospheric plumes, Atmos. Environ. **31**, 991 (1997).

[20] A. Skvortsov and E. Yee, Scaling laws of peripheral mixing of passive scalar in a wall-shear layer, Phys. Rev. E **83**, 036303 (2011).

[21] D. Oettl and E. Ferrero, A simple model to assess odour hours for regulatory purposes, Atmos. Environ. **155**, 162 (2017).

[22] M. Cassiani, P. Franzese, and U. Giostra, A PDF micromixing model of dispersion for atmospheric flow. Part I: development of the model, application to homogeneous turbulence and to neutral boundary layer, Atmos. Environ. **39**, 1457 (2005).

[23] P. G. Moschopoulos, The distribution of the sum of independent gamma random variables, Ann. I. Stat. Math. **37**, 541 (1985).

[24] C. H. Sim, Point processes with correlated gamma interarrival times, Stat. Probabil. Lett. **15**, 135 (1992).

[25] A. M. Mathai, Storage capacity of a dam with gamma type inputs, Ann. Inst. Statist. Math. **34**, 591 (1982).

[26] M. Akkouchi, On the convolution of gamma distributions, Soochow J. Math. **31**, 205 (2005).

[27] T. Stewart, L. Strijbosch, J. Moors, and P. Batenburg, A simple approximation to the convo-

lution of gamma distributions, SSRN Electronic Journal (2007).

[28] S. B. Pope, Turbulent flows (Cambridge Univ. Press, Cambridge, 2011).

[29] M. Cassiani, A. Radicchi, J. Albertson, and U. Giostra, An efficient algorithm for scalar PDF modelling in incompressible turbulent flow; numerical analysis with evaluation of IEM and IECM micro-mixing models, J. Comput. Phys. **223**, 519 (2007).

[30] Z. Warhaft and J. L. Lumley, An experimental study of the decay of temperature fluctuations in grid-generated turbulence, J. Fluid Mech. **88**, 659 (1978).

[31] S. Tavoularis and S. Corrsin, Experiments in nearly homogenous turbulent shear flow with a uniform mean temperature gradient. part 1, J. Fluid Mech. **104**, 311– (1981).

[32] Z. Warhaft, Passive scalars in turbulent flows, Ann. Rev. Fluid Mech. **32**, 203 (2000).

[33] S. Heinz, Statistical mechanics of turbulent flows (Springer Science & Business Media, 2003).

[34] J. Duplat, C. Innocenti, and E. Villermaux, A nonsequential turbulent mixing process, Phys. Fluids **22**, 035104 (2010).

[35] B. L. Sawford and H. Stapountzis, Concentration fluctuations according to fluctuating plume models in one and two dimensions, Boundary-Layer Meteorol. **37**, 89 (1986).

[36] R. Marino, P. Mininni, D. Rosenberg, and A. Pouquet, Inverse cascades in rotating stratified turbulence: fast growth of large scales, Europhys. Lett. **102**, 44006 (2013).

[37] F. Feraco, R. Marino, A. Pumir, L. Primavera, P. Mininni, A. Pouquet, and D. Roesenberg, Vertical drafts and mixing in stratified turbulence: Sharp transition with froude number, Eur. Phys. Lett. **123**, 44002 (2018).

[38] A. Pouquet, D. Rosenberg, and R. Marino, Linking dissipation, anisotropy and intermittency in rotating stratified turbulence, Phys. Fluids **31**, 105 (2019).

[39] D. Buaria, A. Pumir, F. Feraco, R. Marino, A. Pouquet, D. Rosenberg, and L. Primavera, Single-particle lagrangian statistics from direct numerical simulations of rotating-stratified turbulence, Phys. Rev. Fluids **5**, 064801 (2020).